PROCEEDINGS OF SCIENCE

Interpreting the activity of blazar PKS 0735+178 with particle interactions in the jet

Anastasiia Omekiukh,[a,*] **Xavier Rodrigues,**[b,a] **Simone Garrappa,**[c,a] **Vandad Fallah Ramazani ,**[a] **Anna Franckowiak** [a] **and Walter Winter**[d]

[a] *Ruhr University Bochum, Faculty of Physics and Astronomy, Astronomical Institute (AIRUB), Universitätsstraße 150, 44801 Bochum, Germany*

[b] *European Southern Observatory, Karl-Schwarzschild-Straße 2, 85748 Garching bei München, Germany*

[c] *Weizmann Institute of Science, Department of Particle Physics and Astrophysics Herzl Street 234, 76100 Rehovot, Israel*

[d] *Deutsches Elektronen-Synchrotron DESY Platanenallee 6, 15738 Zeuthen, Germany*

E-mail: anastasiia.omeliukh@astro.ruhr-uni-bochum.de

In December 2021, the gamma-ray telescope Fermi-LAT observed the brightest-ever gamma-ray flare from blazar PKS 0735+178. It was also accompanied by activity in optical, ultraviolet and X-rays. Moreover, the IceCube South Pole Neutrino Observatory and Baikal-GVD, a deep underwater neutrino telescope located in Lake Bakal, have both detected neutrinos that were temporally and spatially coincident with PKS 0735+178. This makes this event the first multi-wavelength flare with associated real-time detections by different neutrino observatories. We explain the observed photon and neutrino fluxes in a multi-messenger context with leptohadronic models where they originate from high-energy protons and electrons interacting in the jet. We explore the time-dependent evolution of the parameters based on the observed multi-wavelength spectra. We develop a new approach to explore the parameter space of the models and find multiple solutions with different physical parameters. We discuss the model results and how they improve our understanding of this blazar as a multi-messenger source.

38th International Cosmic Ray Conference (ICRC2023)
26 July - 3 August, 2023
Nagoya, Japan

ICRC2023
38th International Cosmic Ray Conference
The Astroparticle Physics Conference

*Speaker

PoS(ICRC2023)1528

1. Introduction

Blazars are a sub-class of active galactic nuclei (AGN) with a relativistic jet pointing close to the observer's line of sight. Due to highly energetic particles emitting radiation in the jets, they are considered good candidates for cosmic ray and neutrino production sites.

In December 2021, the Fermi Large Area Telescope (Fermi-LAT) observed an unusual activity of the blazar PKS 0735+178 [1]. The gamma-ray flare was characterized by the highest ever detected flux level from this source. The source was also active in optical, ultraviolet and X-rays [2–5].

During the flare, multiple neutrinos were detected by different experiments. On the 8th of December 2021 at 20:02:51.1 UT, the IceCube real-time alert system [6] detected a 172 TeV track-like event with a 30% probability of being an astrophysical neutrino [7]. Almost 4 hours after the IceCube event, Baikal-GVD reported the detection of 43 TeV cascade event with a probability of $\sim 50\%$ to be an astrophysical neutrino [8]. Additionally, 4 days prior to the IceCube event, Baksan Underground Scintillation Telescope detected a muon neutrino with an energy above 1 GeV [9] consistent with the direction of neutrinos detected by IceCube and Baikal-GVD. All three neutrinos point to the same region of the sky with PKS 0735+178 being slightly outside IceCube's 90% localization error but within larger Baikal-GVD and Baksan Underground Scintillation Telescope error contours. This makes this event the first multi-wavelength flare with associated real-time detections by different neutrino observatories.

We investigate the observed neutrino and photon fluxes within the one-zone radiative model paradigm (see also [10–12]) and trace the evolution of the model parameters during the flare duration.

PKS 0735+178 is a BL Lac object with an unknown redshift. We assume redshift $z = 0.45$ based on the analysis presented by [13].

2. Spectral energy distributions

The γ rays measured by Fermi-LAT (E>100 MeV) and neutrino observations were accompanied by follow-up measurements with the following telescopes: Swift-XRT (soft X-rays), Swift-UVOT (optical-UV), Tuorla blazar monitoring program (optical R-band), KAIT (optical R-band), REM (optical, [2]), NOT (optical, [2]), Guillermo Haro Observatory (infra-red, [3]), Metsahovi (radio, 37 GHz) and Mojave (radio, 15 GHz).

We select time periods for building spectral energy distributions based on the source activity in the gamma-ray band as shown in Table 1.

Blazar state	Date	MJD
Quiescent	Jan 23 – Feb 2, 2010	55219 – 55233
Neutrino arrival	Dec 8 – 11, 2021	59556 – 59559
γ flare peak	Dec 17 – 19, 2021	59565 – 59567
Post flare	Dec 25, 2021 – Jan 6, 2022	59573 – 59600

Table 1: Selected time periods for SEDs.

3. Method

We assume that the observed photon and neutrino fluxes originate from the emission of highly energetic particles inside a compact zone (blob) in the jet. To investigate this hypothesis, we use the time-dependent code AM^3 [14] for simulating the radiation processes and interactions undergone by electrons and protons accelerated in the jet. AM^3 employs numerical techniques to solve the system of differential equations governing the evolution of the particle and photon spectra, ensuring a fully time-dependent and self-consistent treatment.

Optical and gamma-ray emission is typically well-explained by leptonic processes even if protons are co-accelerated in the jet (e.g. [10, 14]). Therefore, to find the parameters of the leptohadronic model, we start with the constraining of leptonic parameters. For this, we use the simplest one-zone leptonic model where all electromagnetic radiation is explained exclusively by leptonic processes. At this point, we consider X-rays as upper limits, so only near-infrared, optical, UV, and GeV gamma-ray data points are fitted. We assume that electrons are accelerated to a simple power-law spectrum[1] $dN/d\gamma'_{\rm e} \propto \gamma'^{-\alpha_{\rm e}}_{\rm e}$ with spectral index $\alpha_{\rm e}$, spanning a range of Lorentz factors from $\gamma'^{\rm min}_{\rm e}$ to $\gamma'^{\rm max}_{\rm e}$. The energy spectrum of the electrons is normalized to the total electron luminosity parameter, $L'_{\rm e}$. These particles are then injected into a single spherical blob of size R' (in the comoving frame of the jet) moving along the jet with Lorentz factor Γ, where there is a homogeneous and isotropic magnetic field of strength B' .

To explore the 7-dimensional parameter space of the leptonic models, we do a simple grid scan probing 10 points per dimension resulting in 10 million simulated models. We select the best-fit models by calculating the reduced χ^2 as follows:

$$\chi^2 = \frac{1}{N - N_{\rm par} + 1} \sum_i \frac{(F_i^{\rm data} - F_i^{\rm model})^2}{\sigma_i^2}, \tag{1}$$

where N is the number of data points, $N_{\rm par}$ is the number of free parameters in the model (7 in leptonic, 11 in leptohadronic), $F_i^{\rm data}$ are measured photon fluxes, $F_i^{\rm model}$ the model-predicted photon fluxes, and σ_i the measurement error for the data. After the location of the best fits is roughly defined, we perform local minimization in the region between the closest neighbors to the best fit found in the grid scan using the `iminuit` package [15].

As a next step, we repeat the simulation injecting both electrons and protons with power-law energy distributions. This adds four additional parameters to the model (power-law index α_p, proton minimal and maximal Lorentz factors $\gamma'^{\rm min}_{\rm p}$,$\gamma'^{\rm max}_{\rm p}$, and proton luminosity $L'_{\rm p}$). We perform the next grid scan in a way that leptonic parameters are fixed to the values from the leptonic models while hadronic parameters have 10 values per dimension. The leptohadronic model for each SED requires 10^4 simulations. This time we include all available data into reduced χ^2 except radio[2]. Similarly to the leptonic parameters grid scan, we locally optimize the best solutions afterward.

[1] Parameters with or without prime refer to the values in the jet or observer's frame correspondingly.

[2] Radio fluxes cannot be explained within one-zone models since the typical size of the emission regions seen directly in radio observations is much larger than the blob sizes in one-zone models.

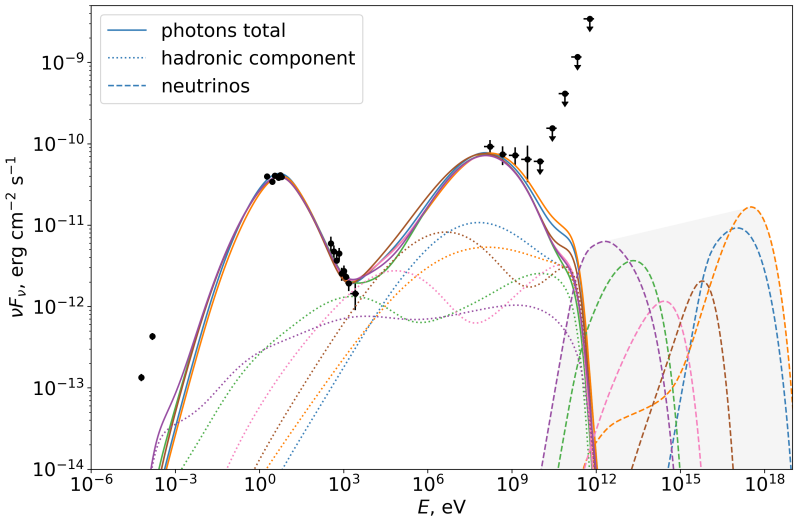

Figure 1: The data points represent multi-wavelength observations of PKS 0735+178 in the time period surrounding the IceCube detection coincident with the source. The solid curves show the total multi-wavelength fluxes predicted by the leptohadronic model assuming six different sets of model parameters, according to Table 2. The dotted curves show the fraction of those fluxes that originate in cascades triggered by hadronic interactions. The dashed curves show the predicted neutrino fluxes for each case, computed self-consistently. As we can see, hadronic interactions can contribute significantly to the observed X-ray fluxes; yet, the parameters of the leptohadronic model cannot be uniquely determined by fitting a model to observations.

4. Results

4.1 Degeneracy of hadronic contributions

The results of a grid scan indicate the existence of a family of solutions that can fit the data equally well. Figure 1 shows different leptohadronic fits to the observed data in the period surrounding the neutrino arrival. All shown models have close values of goodness-of-fit (less than 0.05 difference in reduced χ^2). The solid curves correspond to electromagnetic radiation. The dotted curves represent the contribution of the hadronic process in total photon fluxes, and the dashed curves represent the predicted all-flavor neutrino spectra.

$\log_{10}\gamma'^{p}_{min}$	$\log_{10}\gamma'^{p}_{max}$	α_p	$\log_{10} L'_p$, erg/s
7.0	9.0	3.2	44.55
1.0	9.0	2.5	47.17
1.0	4.9	2.0	48.3
1.5	5.7	1.8	46.85
2.5	6.7	1.5	45.5
1.0	4.9	2.8	50.1

Table 2: Value of hadronic parameters of the models shown in Fig.1. The leptonic parameters are fixed to $R' = 10^{15.55}$, $B' = 2.28$ G, $\Gamma = 15$, $\gamma'^{e}_{min} = 10^{3.5}$, $\gamma'^{e}_{max} = 10^{4.2}$, $\alpha_e = 2.45$, $L'_e = 10^{42.6}$ erg/s.

Different colors correspond to the different values of hadronic parameters. Since the hadronic

contribution is subdominant, multiple shapes of spectra from hadronic cascades can fit the data. Different injection spectra also result in various shapes of neutrino energy spectra. Thus, the prediction of the expected neutrino rates can vary greatly. The shaded area is an area between the lowest-peaked neutrino spectrum and the highest-peaked. Since the parameters are continuous, we expect all possible neutrino spectra to be within this area.

4.2 Best-fit leptohadronic solutions

The degeneracy of hadronic contributions makes it impossible to have exact predictions of the neutrino rates in neutrino observatories. We now consider an optimistic scenario and find those models where neutrino rates are maximized in IceCube.

Fig. 2 shows the best-fit solutions that yield the maximum neutrino event rate in IceCube for each of the observation periods listed in Table 1. The best-fit model parameters as well as neutino rates, are shown in Table 3. As we can see, the predicted multi-wavelength fluxes (solid curves) explain well the optical, X-ray and gamma-ray data. In all cases, the X-ray spectrum benefits from a component originating in hadronic interactions (dotted curves). On the other hand, the optical and gamma-ray peak are described here with only leptonic emission. In particular, during the neutrino arrival, as shown in the lower right panel labeled *(d)*, we can see that the hadronic cascade emission helps reproduce not only the flux level but also the non-trivial spectral shape of the X-ray spectrum.

The corresponding neutrino spectra, which are self-consistently calculated as described in the previous section, are shown as dashed curves. We see that during the quiescent state (upper right panel labeled *(a)*), the model predicts the lowest neutrino flux. The extent of hadronic interactions is limited by the low X-ray fluxes, leading to this weak neutrino production. The predicted neutrino fluxes are highest for the time period surrounding the neutrino arrival, both in panels *(b)* and *(c)*. Finally, in the state immediately following the flare, shown in panel *(d)*, the neutrino flux decreases again, but is still higher than in the quiescent state.

One interesting aspect is that the best-fit size of the blob (R', upper left panel) changes from one epoch to another (see Table 3, second column). During the quiescent state the blob is as large as 10^{17} cm, while during the neutrino arrival and gamma-ray flare peak it is more than an order of magnitude smaller. One possible interpretation of this result is that the gamma-ray flare and the associated neutrino emission may have occurred in a different zone compared to that responsible for the quiescent-state emission of the blazar. Being more compact, this zone possesses higher target photon densities, leading to a temporary increase in both inverse Compton scattering and photohadronic processes.

Similarly, the magnetic field strength also increases sharply during the neutrino arrival compared to the quiescent state, and so does the bulk Lorentz factor (columns two and three of Table 3) . This again suggests different conditions of the environment responsible for the gamma-ray and neutrino-emitting event.

Based on the predicted neutrino spectra, we can then calculate the neutrino events rates N_ν as

$$N_\nu = \frac{1}{3} \cdot T \cdot \int \Phi_\nu(E) A_{\rm eff}(E, \theta) dE, \tag{2}$$

where $A_{\rm eff}(E, \theta)$ is the effective area of the neutrino detector which depends on the neutrino energy and source declination, $\Phi_\nu(E)$ is the all-flavor neutrino flux and T is the exposure time. A coefficient

1/3 is introduced to account for neutrino mixing during the propagation while the detection usually happens only via one channel. We calculate the muon neutrino event rates in IceCube using the experiment's effective area [16]. For the exposure time, we use the different flare periods as follows: beginning of the flare (neutrino arrival SED) – 15 days, gamma flare peak – 8 days, and post flare – 27 days.

Blazar state	R'	B'	Γ	γ'^{e}_{min}	γ'^{e}_{max}	α_e	L_e	γ'^{p}_{min}	γ'^{p}_{max}	α_p	L_p	N_ν
Quiescent	17.17	0.12	6.0	3.85	4.7	2.9	43.7	2.0	6.0	1.5	48.0	0.04
Neurino arrival	15.55	2.28	15.0	3.5	4.2	2.45	42.6	1.0	4.9	2.0	48.3	0.03
γ flare peak	15.54	0.96	17.0	3.0	4.1	1.3	42.7	3.0	4.2	1.3	48.3	0.07
Post flare	16.5	0.08	15.0	3.75	4.5	2.8	42.9	3.5	4.2	1.3	49.8	0.07

Table 3: Best-fit model parameters and neutrino rates in IceCube (exposure time 1 year for the quiescent state, 15 days for the neutrino arrival, 8 days for the gamma flare peak, 27 days for the post flare period).

We predict 0.04 neutrino events per year for the quiescent state under the condition of maximization of neutrino fluxes. During the whole December 2021 - January 2022 flare (which lasted 50 days) we obtain 0.2 neutrino events in total. This is compatible with the detection of one neutrino event in IceCube during the flare.

The difference between neutrino rates in quiescent and flaring states in this optimistic scenario shows that this source becomes a powerful neutrino emitter only during an active state with the neutrino rates being 40 times higher taking the same exposure time. At the same time, the maximum value of neutrino events during the quiescent state, 0.04 year^{-1}, indicates that this source was unlikely to be detected in the IceCube during this state and does not contradict the IceCube analysis of 10 years of data (2008 – 2018) predicting zero neutrinos from the direction of PKS 0735+178 [17].

5. Conclusion

We have explained the emission of the gamma-ray blazar PKS 0735+178, from which direction a high-energy muon neutrino was detected by the IceCube experiment simultaneously with an unprecedented gamma-ray flare of teh source. To explain both multi-wavelength and neutrino observations, we have tested a one-zone leptohadronic model, calculated using a time-dependent numerical approach.

We fitted multi-wavelength observations of the source in four different epochs: a quiescent state, the neutrino arrival time, the peak of the gamma-ray flare, and the state following the flare. By performing a grid scan of the parameter space of the model, we were able to constrain the physical parameters of the emission region and predict their time evolution between the four epochs. We conclude that in all four epochs, electron emission can describe approximately the optical and gamma-ray fluxes. At the same time, electromagnetic cascades triggered by proton interactions can help describe the X-ray fluxes in all four observations epochs.

By comparing the parameter values between the four states, we have shown that the gamma-ray and neutrino observations require a temporary increase in the speed of the emitting region and the magnetic field strength, together with a reduction in the size of the emitting region.

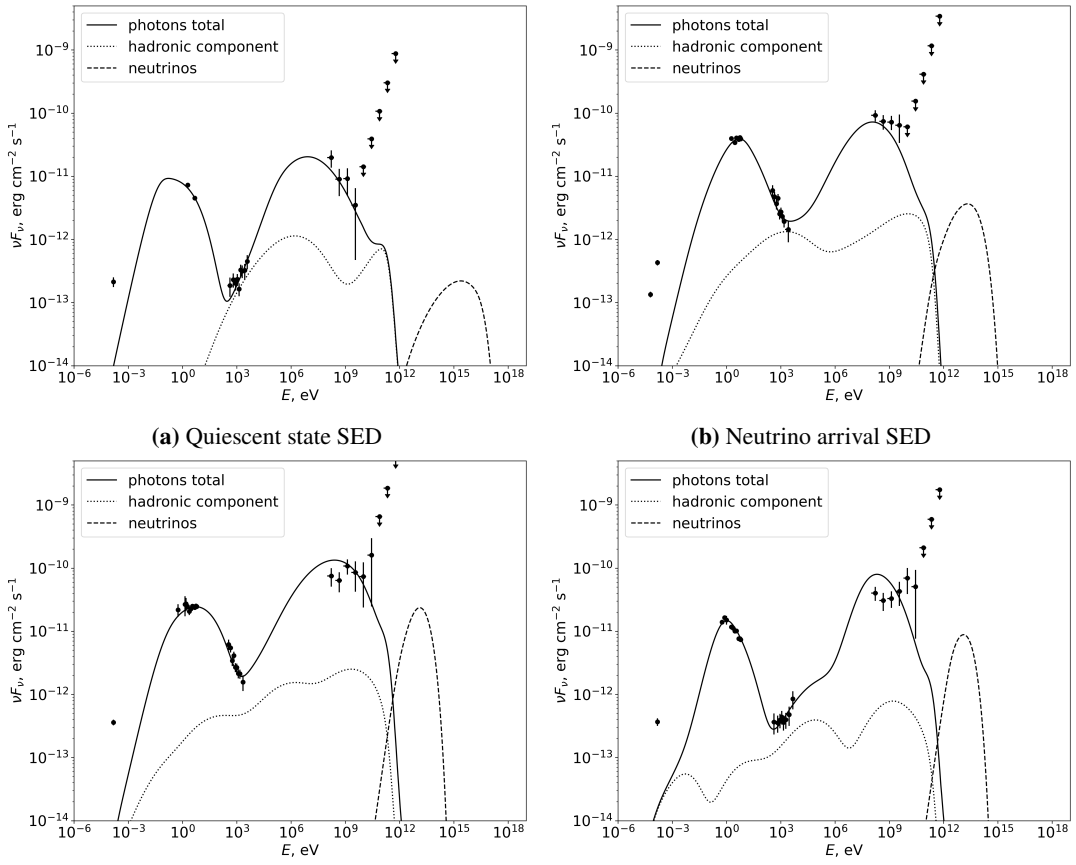

(a) Quiescent state SED

(b) Neutrino arrival SED

(c) Gamma flare peak SED

(d) Post flare SED

Figure 2: Best fit SEDs with one-zone leptohadronic model.

To obtain a relatively high number of neutrino events, the model requires high proton luminosity of the order of 10^{48} erg/s which is an order of magnitude higher than Eddington luminosity for this source. For the after-flare SED the proton luminosity reaches almost 10^{50} erg/s; however, the maximum proton energy becomes lower.

When maximizing the neutrino rates in IceCube during the flare, we obtain a prediction of 0.2 neutrino events. This number is compatible with the one observed within Poisson statistics, as well as with previous leptohadronic models of this source [10–12].

Finally, we have demonstrated the degeneracy in the hadronic parameters when fitting multi-wavelength data. We showed that the hadronic contribution to the total emission, which should mainly reflect on the X-ray fluxes, can be well reproduced with a wide range of proton energies and luminosities, leading to a wide range of expected neutrino peak energies and fluxes.

Breaking the degeneracy of hadronic contributions could be achieved, for example, through a direct measurement of the emitted neutrino energy, as illustrated in Figure 1. This could be possible with higher neutrino statistics, to which will contribute the next-generation neutrino telescopes such as IceCube-Gen2 [18] and KM3NeT [19].

While this work provides a description of the time evolution of the source parameters, this was only possible for four epochs, mainly due to the scarcity of X-ray data. In that sense, continued

multi-wavelength monitoring of the source will be crucial to eventually resolve the degeneracy in the hadronic parameters.

Finally, TeV measurements with future instruments such as CTA [20], as well as in MeV gamma rays with experiments that are currently being proposed, will allow us to complete our multi-wavelength picture of this blazar and better understand its nature as a cosmic-ray accelerator and a neutrino source.

References

[1] S. Garrappa, S. Buson, J. Sinapius, and M. Kadl *The Astronomer's Telegram* **15099** (Dec., 2021) 1.

[2] E. Lindfors, T. Hovatta, T. Pursimo, V. Pinter, S. Warren, T. Andradi-Brown, Z.-L. Xie, E. Banados, D. Fugazza, and E. Molinari *The Astronomer's Telegram* **15136** (Dec., 2021) 1.

[3] L. Carrasco, E. Recillas, G. Escobedo, A. Porras, V. Chavushyan, and Y. D. Mayya *The Astronomer's Telegram* **15148** (Dec., 2021) 1.

[4] M. Santander and S. Buson *The Astronomer's Telegram* **15102** (Dec., 2021) 1.

[5] S. Haemmerich, A. Zainab, A. Gokus, P. Weber, I. Kreykenbohm, and J. Wilms *The Astronomer's Telegram* **15108** (Dec., 2021) 1.

[6] IceCube Collaboration *Astroparticle Physics* **92** (Jun, 2017) 30–41.

[7] IceCube Collaboration *GRB Coordinates Network* **31191** (Dec., 2021) 1.

[8] Z. A. Dzhilkibaev, O. Suvorova, and Baikal-GVD Collaboration *The Astronomer's Telegram* **15112** (Dec., 2021) 1.

[9] V. B. Petkov, Y. F. Novoseltsev, R. V. Novoseltseva, and Baksan Underground Scintillation Telescope Group *The Astronomer's Telegram* **15143** (Dec., 2021) 1.

[10] N. Sahakyan, P. Giommi, P. Padovani, M. Petropoulou, D. Bégué, B. Boccardi, and S. Gasparyan **519** no. 1, (Feb., 2023) 1396–1408.

[11] R. Prince, S. Das, N. Gupta, P. Majumdar, and B. Czerny *arXiv e-prints* (Jan., 2023) arXiv:2301.06565.

[12] VERITAS Collaboration, H.E.S.S. Collaboration, K. Mori *arXiv e-prints* (June, 2023) arXiv:2306.17819.

[13] K. Nilsson, T. Pursimo, C. Villforth, E. Lindfors, L. O. Takalo, and A. Sillanpää *Astronomy &amp Astrophysics* **547** (Oct, 2012) A1.

[14] S. Gao, M. Pohl, and W. Winter *The Astrophysical Journal* **843** no. 2, (Jul, 2017) 109.

[15] H. Dembinski et al., July, 2023. `https://doi.org/10.5281/zenodo.8191656`.

[16] IceCube Collaboration *The Astrophysical Journal* **835** no. 2, (Feb., 2017) 151.

[17] IceCube Collaboration *Phys. Rev. Lett.* **124** (Feb, 2020) 051103.

[18] IceCube Collaboration *Journal of Physics G: Nuclear and Particle Physics* **48** (06, 2021) 060501.

[19] KM3NeT Collaboration *Astroparticle Physics* **111** (2019) 100–110.

[20] Cherenkov Telescope Array Consortium, *Science with the Cherenkov Telescope Array*. 2019.

PoS(ICRC2023)1528